Environ. Sci. Technol. **2006**, *40,* 6104−6109

Fabrication and Characterization of Silica/Titania Nanotubes Composite Membrane with Photocatalytic Capability

HAIMIN ZHANG, XIE QUAN,* SHUO CHEN, AND HUIMIN ZHAO

School of Environmental and Biological Science and Technology, Dalian University of Technology, Dalian 116024, China

Silica/titania nanotubes composite membranes were successfully prepared from silica/titania sols using porous alumina support membranes. XRD patterns of the composite membranes confirmed that the embedding of amorphous silica into nanophase titania matrix helped to increase the thermal stability of titania which suppressed the phase transformation from anatase to rutile and decreased the size of titania particles. Ninety-five percent of the pore volume of composite membrane was located in mesopores with diameters ranging from 1.4 to 10 nm. The surface of these composite membranes exhibited extremely high affinity for water under UV irradiation with water contact angle decreased from 62° to nearly 5° within 80 min. By coupling membrane separation with photocatalysis technique, the removal efficiency of Direct Black 168 was improved remarkably; being 85% within 100 min, while the values were 66% and 73% with photocatalysis alone or membrane separation alone during the same time, respectively. Good photocatalytic activity and wettability of composite membrane under UV irradiation helped to obtain high permeate flux across the composite membrane. The silica/titania nanotubes composite membrane had the multifunctions of separation, degradation, and improvement of membrane flux in photooxidation of organic contaminants in wastewater.

Introduction

Membrane separation is an emerging technology with advantages of low energy costs, potential material recovery, low environmental impact, and possible integrated processes with selective removal of certain components (*1*, *2*). Membrane separation processes are suitable for application in many fields such as the textile industry (*3*), food and pharmaceutical industry, and wastewater recycling (*4*). However, this method only transfers pollutants from one phase to another without any degradation.

TiO_2 nanostructures have become a focus of considerable interest over the past several years because they possess some unique properties relevant to the applications, including chemical sensing (*5*−*7*), photocatalysis (*8*, *9*), and photovoltaics (*10*−*12*). TiO_2 photocatalysis proves to be a promising technology for the purification and treatment of both contaminated air and water (*13*). Chen and co-workers have reported a novel TiO_2-based p−n junction nanotube with excellent photoactivity (*14*). Some multicomponent or mixed oxides such as TiO_2/ZrO_2, $Ni_2O_3/TiO_{2-x}B_x$, $K_2La_2TiO_3$, and SiO_2/TiO_2 exhibit good photoactivity (*15*−*17*), but the separation of powder photocatalysts is difficult because of their fine sizes. Several researchers have attempted to combine photocatalysis with membrane separation technique using TiO_2 powder photocatalyst for removal of organic pollutants from water. In their research, suspended TiO_2 powder photocatalyst was separated successfully by ultrafiltration or microfiltration after photocatalytic reaction, but photocatalysis and membrane separation were two independent operation processes. This approach increased not only the complexity of practical application (*18*, *19*), but also fouling of the filtration membrane because of fine TiO_2 particles choking the pores. Moreover, powder photocatalysts were easily lost in the process of photocatalytic reaction and separation. Molinari and co-workers tried to degrade toxic organic species such as 4-nitrophenol using TiO_2 powder photocatalysts and organic membranes, but the organic membranes are prone to destruction by UV irradiation (*20*, *21*).

Before applying the photocatalysis and membrane separation techniques in water treatment, the issues of membrane fouling, powder photocatalysts loss, and separation must be addressed properly. It is possible to solve these problems using ceramic composite membranes with photocatalytic capability. Ceramic membranes are UV light resistant. When these membranes are used in combination with photocatalysis, stable permeate fluxes can be achieved without membrane damage. Some researchers indicated that photocatalysis prevented foulants from adhering to the membrane surface, thus decreasing membrane fouling (*22*). This work focuses on the fabrication of silica/titania nanotubes composite membranes with photocatalytic capability. The composite membranes may be important for improving membrane flux and preventing membrane from fouling.

Experimental Section

All of the reagents (analytical grade purity) were purchased from Tianjin Kermel Chemical Reagents Development Centre and were used without further purification. The porous alumina support membranes with 200 nm diameter pores are disk-shaped,the diameter is 47 mm, and the thickness is 50 μm, and they were purchased from Whatman Anopore Filters.

Preparation of Silica/Titania Nanotubes Composite Membranes. Silica/titania nanotubes composite membranes were prepared using the sol−gel method. In order to obtain 20/80 silica/titania sol in mole percent (20/80 silica/titania is denoted 20%-silica/titania in the following depiction), the following procedure was performed: 23.5 mL of $Ti(Oi-C_3H_7)_4$ and 4.5 mL of $Si(OC_2H_5)_4$ were added to 23 mL of ethanol, and the resulting solution was stirred for 30 min at room temperature. A mixture of 23 mL of ethanol and 18 g of 4.4 mol/L HCl aqueous solution was added slowly to the above mixed solution.

The resulting mixture was allowed to undergo hydrolysis reaction at room temperature for 60 min. Afterward, it was placed in an ultrasonic cleaning bath for 10 min resulting in a transparent straw-color silica/titania sol. The alumina support membrane was immediately dipped into this solution. After the desired immersion time, the membrane was removed from the sol and dried in air for 1 h at room temperature. The membranes and correspondingly dried silica/titania sol were then placed in a muffle furnace. The

* Corresponding author phone:+86-411-84706140; fax:+86-411-84706263; e-mail: quanxie@dlut.edu.cn.

10.1021/es060092d CCC: $33.50
Published on Web 08/30/2006

temperature was ramped to 400 °C (100 °C/h) and kept at 400 °C for 2 h before ramped back down (50 °C/h) to room temperature.

Instruments and Analysis Methods. The morphology of silica/titania composite membranes and silica/titania nanotubes was observed using a scanning electron microscope (SEM, JSM-5600LV, Oxford, UK) and a transmission electron microscope (TEM, Tecnai G^2 20, Japan). The phases of silica/titania composite membranes were identified by X-ray diffractometer (XRD, LabX-6000, Shimadzu, Japan). IR-spectra of silica/titania composite were measured to investigate structural information and specific molecule-groups information (IR Prestige-21, Fourier transform spectrophotometer, Shimadzu, Japan). The zeta-potential of silica/titania powder was measured using a zeta-potential analyzer (Zetaplus V3.52 Japan). UV−visible diffuse reflectance spectra (DRS) and concentration of Direct Black 168 were determined by a UV−Vis spectrophotometer (JASCO V-550, Japan). The prepared silica/titania composite membranes were characterized using a nitrogen adsorption−desorption measurement (NOVA 4200e, surface area and pore size analyzer) to examine the pore structure. The surface wettabilities of silica/titania nanotubes composite membranes were measured using a contact angle meter (CA-C, Kyowa Surface Science).

Membrane Permeability, Rejection, and Photocatalytic Experiments. All permeability and rejection measurements were evaluated using 20%-silica/titania composite membranes in the membrane test unit. The whole evaluation system was a circling flow system. The dye Direct Black 168 (molecular weight of 734 g/mol and molecular structure with 2.0 nm width, 0.11 nm depth, and 0.57 nm thickness) solution was pumped from a solution reservoir through the membrane cell and back to the reservoir. Both permeate and retentate were recycled. The temperature of the system was kept at 298 K. The flow rate through test cell was kept at 12.7 L/h.

Photocatalytic reaction experiments of silica/titania nanotubes composite membranes were conducted in the same membrane test unit. A 1000 mL portion of 50 mg/L Direct Black 168 was used as model polluting agent. When the photocatalytic reaction was performed, a 300 W high-pressure mercury lamp with a characteristic wavelength of 365 nm was used as UV source, which was surrounded by a quartz cooling thimble (25 mm diameter). The lamp was placed at the top of the reactor with the spacing between the light bulb and the surface of composite membrane being 100 mm. The light intensity at this distance was 400 μW/cm^2. A solution of 3 mL was withdrawn at given reaction intervals, and was quickly returned to the reactor after being analyzed with a spectrophotometer at 610 nm. During the experiment, air was bubbled into the solution using an inorganic ceramic microfiltration membrane. Direct Black 168 solution was stirred by air bubbling in darkness for 30 min to establish adsorption−desorption equilibrium before the experiments started.

Results and Discussion

X-ray Diffraction Analysis. Figure 1 shows XRD patterns of the prepared 20%-silica/titania composite membranes at different calcination temperatures and titania composite membrane at 400 °C. For 20%-silica/titania composite membranes, the dominant phase of the titania was anatase. No significant peaks of rutile, brookite, or silica crystal were observed for all calcination temperatures as shown in Figure 1. For titania composite membrane, significant peaks of rutile phase and brookite phase were observed clearly at 400 °C. It was confirmed that the 20%-silica/titania composite had high thermal stability that suppressed the phase transformation of titania from anatase to rutile (*23*, *24*). The size of the crystallites can be estimated from the broadening of corresponding X-ray diffraction peaks using the Scherrer

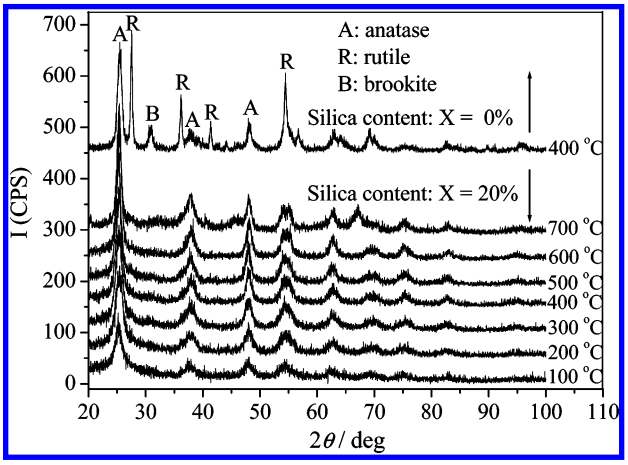

FIGURE 1. XRD patterns of 20%-silica/titania composite membranes at different calcination temperatures and titania composite membrane at 400 °C.

TABLE 1. Crystallite Size of Titania

	20%-silica/titania						
T (°C)	100	200	300	400	500	600	700
crystallite size (nm)	5.5	5.5	5.9	6.8	8.0	8.3	9.3

	calcination at 400 °C			
samples	0%	20%	33%	50%
(*X*-silica/titania)	(pure titania)			
crystallite size (nm)	23	6.8	6.8	7.0

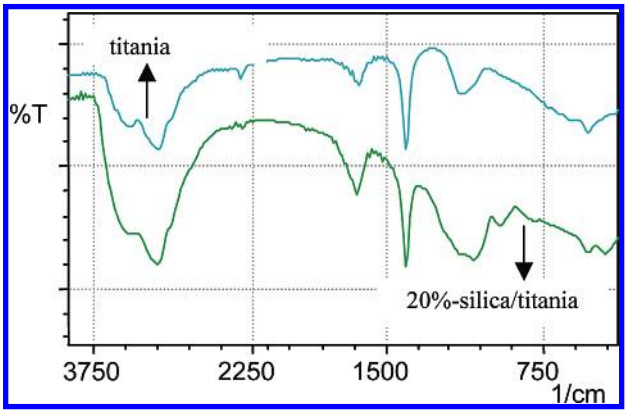

FIGURE 2. FT−IR spectra of titania and 20%-silica/titania particles calcined at 400 °C for 2 h.

formula. Table 1 shows the crystallite sizes of silica/titania. For 20%-silica/titania composite, the crystallite size of titania increased with increasing calcination temperature. However, there was no significant change in the crystallite size of silica/titania particles with changing the silica contents (except pure titania). The above results confirmed that the embedding of some portion of silica into titania particles inhibited the growth of anatase crystal of titania particles. The small titania particles with anatase phase were very beneficial for the formation of silica/titania nanotubes composite membrane with photocatalytic capability.

FT−IR Spectroscopy Analysis. Figure 2 shows FT−IR spectra of 20%-silica/titania mixture. It was reported that the high-frequency part of the spectra was dominated by the OH stretching (3100−3500 cm^{-1}) and bending (1640 cm^{-1}) of water (*25*, *26*). Compared with pure titania, this water band of 20%-silica/titania increased when the silica was embedded into titania particles. For titania and 20%-silica/titania, the deformation modes of CH− stretching modes of alcohol groups from the alkoxide appeared in the range between 1300 and 1500 cm^{-1} (*27*). The band at 1100 cm^{-1}

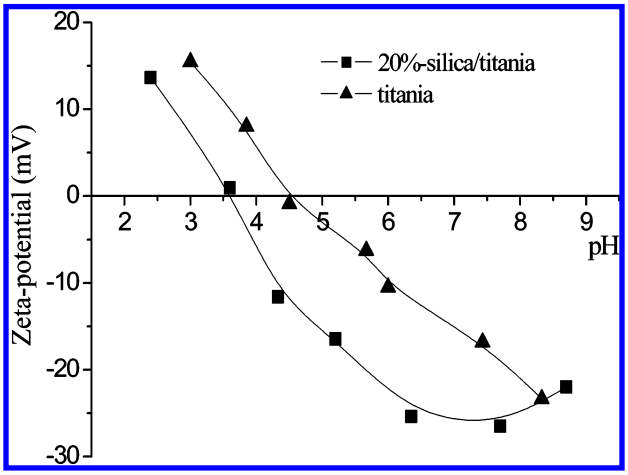

FIGURE 3. Plot of the zeta-potential as a function of pH for 20%-silica/titania and titania suspension (0.1 g/L) in the presence of KNO_3 (10^{-3} mol/L).

could be attributed to Ti(O−C)−stretching vibration (*27*) and the C element could be from $Ti(Oi-C_3H_7)_4$. For 20%-silica/titania, the peaks at wavenumber near 1074 cm^{-1} and 930−970 cm^{-1} corresponded to the stretching vibration of Si−O−Si and Ti−O−Si, respectively (*28*, *29*). The peaks at wavenumber near 800 and 460 cm^{-1} were due to Si−O−Si symmetry stretching vibration and bending vibration (*24*, *30*). Heat treatment of the gels (titania and 20%-silica/titania) at 400 °C led to the decomposition of the alkoxide−additive complex and the formation of Ti−O group at a wavenumber near 538 cm^{-1}. The above results illustrated that amorphous silica phase did not exist as a segregated phase, but formed partially Ti−O−Si group in the matrix of anatase-phase titania. XPS analysis of 20%-silica/titania demonstrated that the atomic concentration of O1s, Ti2p, C1s, and Si2p was 64.45%, 15.03%, 16.49%, and 4.03%, respectively. The atomic ratio of silicon and titanium in silica/titania was about 1:3.7.

Zeta-Potential of Silica/Titania Analysis. Figure 3 shows the electrophoretic mobility data at different values of pH for the suspensions of titania and 20%-silica/titania particles. The isoelectric point of 20%-silica/titania is 3.6 pH units, which is lower than 4.5 pH units for that of titania. Moreover, the isoelectric points of 20%-silica/titania and titania are both lower than 6.2 pH units, the value of Degussa P-25 (*31*), resulting in the equilibrium in eq 1 shifting to the left. Kiwi et al. (*32*) and Boehm et al. (*33*) have demonstrated the presence of the processes (eqs 1 and 2). The presence of surface acidic groups may result in the lower isoelectric point of 20%-silica/titania. Usually, when pH is lower than 3.6, anionic pollutants are more easily adsorbed by the 20%-silica/titania than cationic pollutants. This adsorption is an important factor for heterogeneously photocatalytic reaction.

$$TiOH_2^+ \rightarrow TiOH + H^+ \quad (1)$$

$$TiOH \rightarrow TiO^- + H^+ \quad (2)$$

Scanning Electron Microscope Analysis. Figure 4a shows a scanning electron micrograph of the surface of 20%-silica/titania composite membrane with immersion time of 10 min. As shown, there are many fine and uniform pores in the membrane. In order to investigate 20%-silica/titania nanotubes microstructures in the inside of composite membrane, one surface layer of the composite membrane was removed, and the membrane was glued to a piece of filter paper with the polished face up. The resulting composite was immersed into 6 mol/L NaOH solution for 5 min at 50 °C to dissolve the alumina, and then rinsed with 1 mol/L HCl and deionized water, respectively. Figure 4b shows SEM and TEM images

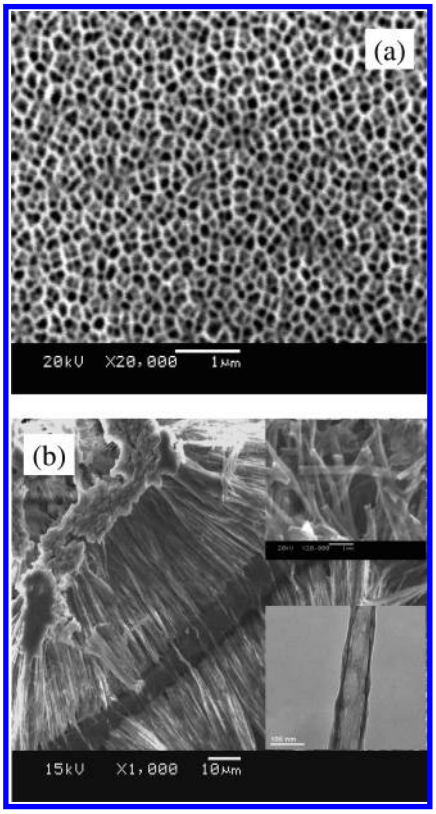

FIGURE 4. Electron photographs of 20%-silica/titania composite membrane and 20%-silica/titania nanotubes prepared in the alumina membranes with 200 nm diameter pores. The sol was maintained at 293 K and the immersion time was 10 min. (a) The surface of 20%-silica/titania composite membrane; (b) 20%-silica/titania nanotubes.

of 20%-silica/titania nanotubes. The 20%-silica/titania nanotubes are about 50 μm long (the thickness of alumina membrane) with outer diameters of 100−200 nm. Most of the nanotubes observed in the SEM investigation are shorter than 50 μm and unordered, which may be attributed to the break of the nanotubes during the preparation of the SEM samples. A typical TEM image is shown in the inset (bottom) in Figure 4b. The 20%-silica/titania nanotubes exhibit the shape of a straight tube. The pore/wall of the nanotube structure can be observed clearly; the outer diameter of the nanotube is about 130 nm and the inner diameter is about 50 nm.

N_2 Adsorption−Desorption Analysis. Figure 5 shows N_2 adsorption−desorption isotherms of the 20%-silica/titania nanotubes composite membrane calcined at 400 °C for 2 h. The isotherm was of type II according to the BDDT classification (*34*). The BET surface area of 20%-silica/titania nanotubes composite membrane was 16.91 m^2/g. The inset in Figure 5 shows the corresponding pore size distribution curve calculated from desorption branch of N_2 isotherm by the BJH method using the Halsey equation. The pore size distribution of composite membrane is correspondingly wide ranging from 1.0 to 60 nm, but 95% of the pore volume is located in mesopores of diameters ranging from 1.4 to 10 nm (*35*). It is these mesopore structures that allow rapid diffusion of products during UV illumination and enhance the rate of photocatalytic reaction, as seen subsequently.

UV−Visible Diffuse Reflectance Spectra Analysis. The UV−vis absorption spectrum of the 20%-silica/titania composite membrane and titania composite membrane indicate the maximum absorption wavelengths are around 260 and 300 nm, respectively (shown in Figure 6). The band gap absorption edges of 20%-silica/titania composite membrane

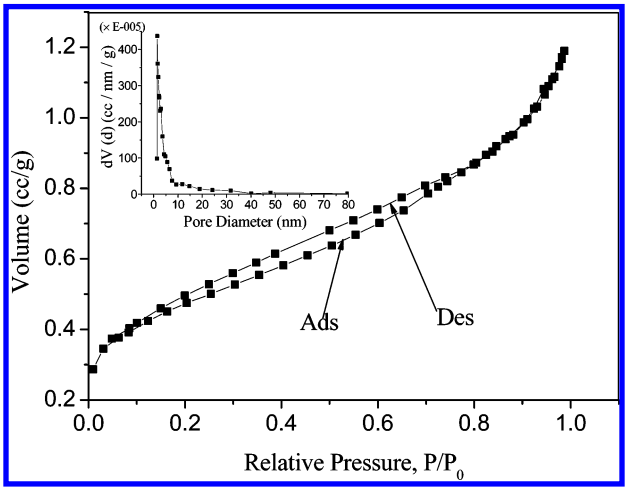

FIGURE 5. N_2 adsorption−desorption isotherm of the 20%-silica/titania composite membrane after calcination at 400 °C for 2 h; the inset is the BJH pore size distribution plot.

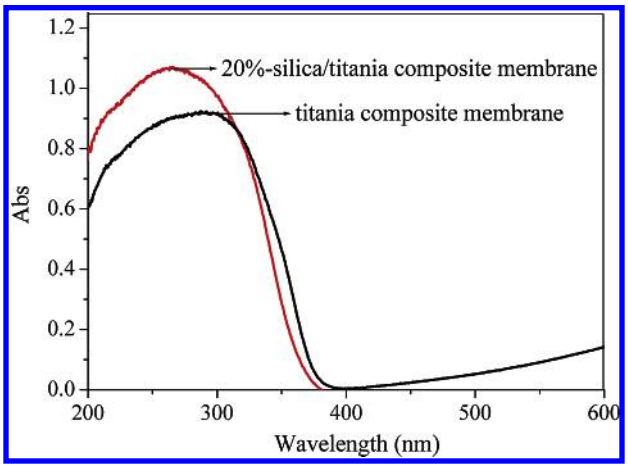

FIGURE 6. Diffuse reflectance UV−vis spectra of the samples calcined at 400 °C for 2 h.

and titania composite membrane are around 375 and 390 nm, and the band gap energies calculated with Kubelka−Munk function (*36*) are about 3.30 and 3.18 eV, respectively. Compared with titania composite membrane, the small blue-shift of 20%-silica/titania composite membrane is mainly due to the formation of small titania particles by embedding of amorphous silica into the titania matrix. The absorption intensity of 20%-silica/titania composite membrane is obviously higher than that of titania composite membrane, which would be beneficial for photocatalytic degradation of organic pollutants under UV irradiation.

Evaluation of Surface Wettability under UV Irradiation. Surface wettabilities were evaluated by water contact angle. Figure 7 shows changes of water contact angle between hydrophilic states and hydrophobic ones for titania composite membrane and 20%-silica/titania composite membrane. Water contact angles of titania composite membrane and 20%-silica/titania composite membrane decreased under UV irradiation from initial values of 72° and 62° to 17° and 5° within 80 min, respectively. After UV irradiation stopped, water contact angles of both composite membranes increased. After 130 min, their water contact angles resumed almost their initial values. The water contact angles of 20%-silica/titania composite membrane before and after UV irradiation were obviously lower than those of titania composite membrane. The above results illustrated that the wettability of composite membrane was improved when some portion of silica was embedded into titania particles.

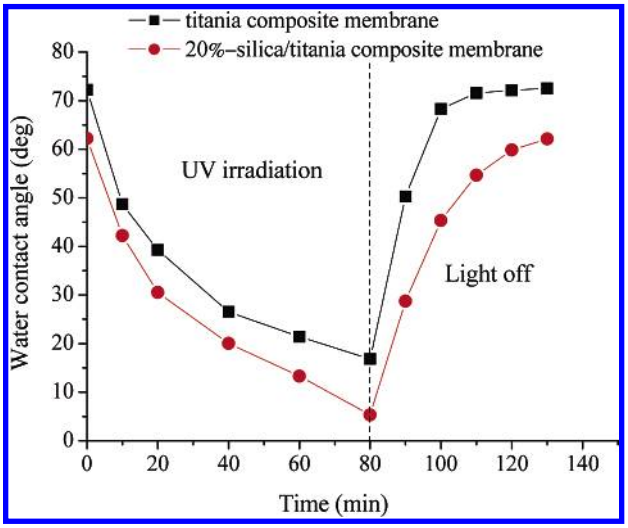

FIGURE 7. Hydrophilic−hydrophobic conversion of titania composite membrane and 20%-silica/titania composite membrane.

This good wettability of 20%-silica/titania composite membrane under UV irradiation would be very important for improving the flux across the composite membrane.

Coupling Photocatalysis and Membrane Separation Experiments with 20%-Silica/Titania Nanotubes Composite Membrane. The preliminarily photocatalytic experiments of silica/titania nanotubes composite membranes with different mol % of silica (0, 11%, 20%, 33%) were performed in a circling flow system. The experimental results demonstrated that the highest removal efficiency of Direct Black 168 was obtained using 20%-silica/titania nanotubes composite membrane. Thus, 20%-silica/titania nanotubes composite membranes were selected for the following experiments. The transmembrane pressure difference of membrane test unit was 0.05 MPa. The Direct Black 168 in water has a strong absorption peak at 610 nm, and it is quite stable under the UV irradiation at λ_{max} = 365 nm (curve a in Figure 8). Curve b in Figure 8 shows that the dye adsorption on the surface of 20%-silica/titania nanotubes composite membrane is only 7% within 100 min. When the 20%-silica/titania nanotubes composite membrane was used as photocatalyst, the dye could be decomposed under UV irradiation, with the removal being 66% within 100 min (curve c in Figure 8). The removal of Direct Black 168 with membrane separation alone reached 73% within 100 min (curve d in Figure 8), and this removal should include two aspects: adsorption (physical and chemical) and mechanical retention. By coupling photocatalysis and membrane separation technique, 85% removal efficiency of Direct Black 168 was achieved within 100 min (curve e in Figure 8). The results implied that the silica/titania nanotubes composite membrane possessed the multifunctions of photocatalysis and separation. SEM image (the image is not given) of the composite membrane after being used 10 times showed that the pores structure and morphology of the composite membrane had no significant change and damage compared with before being used. Many fine and uniform pores in the composite membrane could still be observed after 10 repeated experiments. The COD removal of Direct Black 168 solution under different conditions using 20%-silica/titania nanotubes composite membranes is shown in Figure 9. After 200 min, COD of Direct Black 168 solution decreased 68%, 74%, and 89% under photocatalysis alone, membrane separation alone, and combining photocatalysis with membrane separation, respectively.

Permeability Experiments with 20%-Silica/Titania Nanotubes Composite Membrane. Figure 10 shows Direct Black 168 solutions permeate flux across 20%-silica/titania nano-

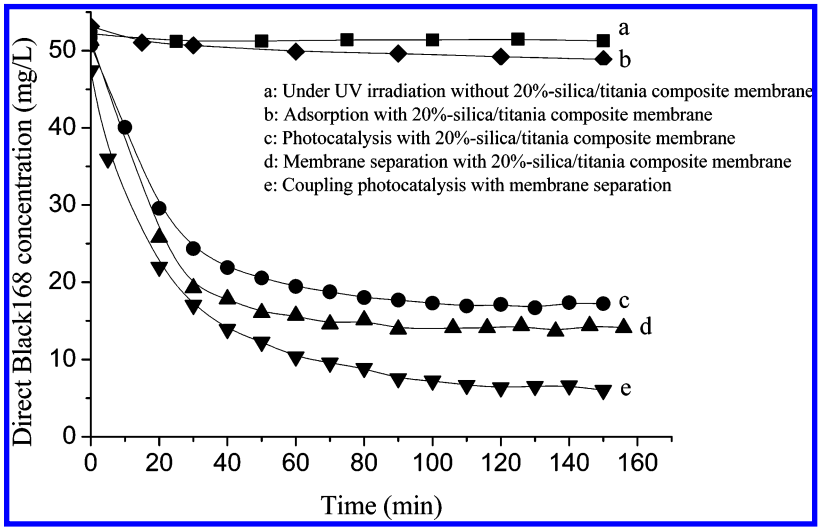

FIGURE 8. Concentration of Direct Black 168 solution versus time under different conditions. $V = 1000$ mL; $T = 298$ K; $C_{feed} = 50$ mg/L; initial pH = 3.5; air flow = 1.0 L/min; $\Delta P = 0.05$ MPa.

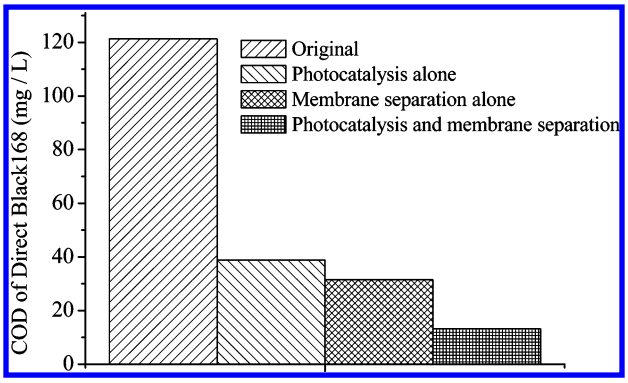

FIGURE 9. COD removal of Direct Black 168 solution under different conditions. $V = 1000$ mL; $T = 298$ K; $C_{feed} = 50$ mg/L; initial pH = 3.5; air flow = 1.0 L/min; $\Delta P = 0.05$ MPa.

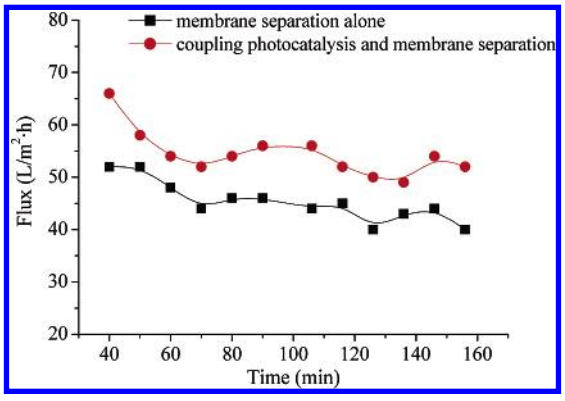

FIGURE 10. Direct Black 168 permeate flux of the 20%-silica/titania composite membrane with and without UV light at pH 3.5; pressure difference 0.05 MPa and Direct Black 168 concentration 50 mg/L.

tubes composite membrane with and without UV irradiation at a transmembrane pressure difference of 0.05 MPa. The permeate flux across composite membrane decreased with time. Nevertheless, after 60 min, membrane filtration alone achieved a steady permeate flux of 44 L/m^2·h. When the composite membrane was used in combination with UV light (photocatalysis), stable permeate flux of 53 L/m^2·h could be achieved without membrane damage. Photocatalysis−membrane filtration resulted in an increase of 9 L/m^2·h permeate flux. This improved permeate flux probably was due to two aspects: good wettability of silica/titania nanotubes composite membrane under UV irradiation, and the photocatalytic degradation of Direct Black 168 that reduces composite membrane fouling. Further investigation is needed for the self-cleaning function of this novel silica/titania nanotubes composite membrane.

According to our research, the silica/titania nanotubes composite membranes had the multifunctions of separation, degradation, and improvement of membrane flux in photooxidation of organic contaminants in wastewater. The improvement of permeate flux across composite membrane under UV irradiation might have important significance for reducing membrane fouling. The self-cleaning function of composite membrane will be further investigated in future work. Coupling the photocatalysis with membrane techniques in a single device boosted the efficiency without excessively increasing the complexity of the process and resulted in a very powerful process with a great innovation in water purification.

Acknowledgments

We thank the National Basic Research Program of China (Project 2003CB415006) and the National Nature Science Foundation of China (Projects 20337020 and 20525723) for financial support.

Literature Cited

(1) Voigt, I.; Fischer, G.; Puhlfürss, P.; Schleifenheimer, M.; Stahn, M. TiO_2− NF-membranes on capillary supports. *Sep. Purif. Technol.* **2003**, *32*, 87−91.

(2) Ahmad, A. L.; Othman, M. R.; Mukhtar, H. H_2 separation from binary gas mixture using coated alumina−titania membrane by sol−gel technique at high-temperature region. *Int. J. Hydrogen Energy* **2004**, *29*, 817−828.

(3) Xu, L.; Li, W. P.; Lu, S. Q.; Wang, Z.; Zhu, Q. X.; Ling, Y. Treating dyeing waste water by ceramic membrane in crossflow microfiltration, *Desalination* **2002**, *149*, 199−203.

(4) Combe, C.; Guizard, C.; Aimar, P.; Sanchez, V. Experimental determination of four characteristics used to predict the retention of a ceramic nanofiltration membrane. *J. Membr. Sci.* **1997**, *129*, 147−160.

(5) Varghese, O. K.; Gong, D. W.; Paulose, M.; Ong, K. G.; Dickey, E. C.; Grimes, C. A. Extreme changes in the electrical resistance of titania nanotubes with hydrogen exposure. *Adv. Mater.* **2003**, *15*, 624−627.

(6) Varghese, O. K.; Gong, D. W.; Paulose, M.; Ong, K. G.; Grimes, C. A. Hydrogen sensing using titania nanotubes. *Sens. Actuators, B* **2003**, *93*, 338−344.

(7) Mor, G. K.; Carvalho, M. A.; Varghese, O. M.; Pishko, M. V.; Grimes, C.A. A room-temperature TiO_2-nanotube hydrogen sensor able to self-clean photoactively from environmental contamination. *J. Mater. Res.* **2004**, *19* (*2*), 628−634.

(8) Livraghi, S.; Votta, A.; Paganini, M. C.; Giamello, E. The nature of paramagnetic species in nitrogen doped TiO_2 active in visible light photocatalysis. *Chem. Commum.* **2005**, *4*, 498−500.
(9) Tang, C.; Chen, V. The photocatalytic degradation of reactive black 5 using TiO_2/UV in an annular photoreactor. *Water Res.* **2004**, *38*, 2775−2781.
(10) Hagfeldt, A.; Gratzel, M. Molecular photovoltaics. *Acc. Chem. Res.* **2000**, *33*, 269−277.
(11) Mor, G. K.; Shankar, K.; Paulose, M.; Varghese, O. K.; Grimes, C.A. Enhanced photocleavage of water using titania nanotube arrays. *Nano Lett.* **2005**, *5* (*1*), 191−195.
(12) Quan, X.; Yang, S. G.; Ruan, X. L.; Zhao, H. M. Preparation of titania nanotubes and their environmental applications as electrode. *Environ. Sci. Technol.* **2005**, *39*, 3770−3775.
(13) Hagfeldt, A.; Gratzel, M. Light-induced redox reactions in nanocrystalline systems. *Chem. Rev.* **1995**, *95*, 49−68.
(14) Chen, Y. S.; Crittenden, J. C.; Hackney, S.; Sutter, L.; Hand, D.W. Preparation of a novel TiO_2-based p−n junction nanotube photocatalyst. *Environ. Sci. Technol.* **2005**, *39*, 1201−1208.
(15) Zhao, W.; Ma, W. H.; Chen, C. C.; Zhao, J. C.; Shuai, Z.G. Efficient degradation of toxic organic pollutants with $Ni_2O_3/TiO_{2-x}B_x$ under visible irradiation. *J. Am. Chem. Soc.* **2004**, *126*, 4782−4783.
(16) Takata, T.; Shinohara, K.; Tanaka, A.; Hara, M.; Kondo, J. N.; Domen, K. A highly active photocatalyst for overall water splitting with a hydrated layered perovskite structure. *J. Photochem. Photobiol., A* **1997**, *106*, 45−49.
(17) Fu, X.; Clark, L. A.; Yang, Q.; Anderson, M.A. Enhanced photocatalytic performance of titania-based binary metal oxides: TiO_2/SiO_2 and TiO_2/ZrO_2. *Environ. Sci. Technol.* **1996**, *30*, 647−653.
(18) Xi, W. M.; Geissen, S. U. Separation of titanium dioxide from photocatalytically treated water by cross-flow microfiltration. *Water Res.* **2001**, *35* (*5*), 1256−1262.
(19) Molinari, R.; Palmisano, L.; Drioli, E.; Schiavello, M. Studies on various reactor configurations for coupling photocatalysis and membrane processes in water purification. *J. Membr. Sci.* **2002**, *206*, 399−415.
(20) Molinari, R.; Mungari, M.; Drioli, E.; Di Paola, A.; Loddo, V. Study on a photocatalytic membrane reactor for water purification. *Catal. Today* **2000**, *55*, 71−78.
(21) Molinari, R.; Grande, C.; Drioli, E.; Palmisano, L.; Schiavello, M. Photocatalytic membrane reactors for degradation of organic pollutants in water. *Catal. Today* **2001**, *67*, 273−279.
(22) Lee, S. A.; Choo, K. H.; Lee, C. H.; Lee, H. I.; Hyeon, T. W.; Choi, W. Y.; Kwon, H. H. Use of ultrafiltration membranes for the separation of TiO_2 photocatalysts in drinking water treatment. *Ind. Eng. Chem. Res.* **2001**, *40*, 1712−1719.
(23) Jung, K. Y.; Park, S. B. Anatase-phase titania: preparation by embedding silica and photocatalytic activity for the decomposition of trichloroethylene. *J. Photochem. Photobiol., A* **1999**, *127*, 117−122.
(24) Jung, K. Y.; Park, S. B. Enhanced photoactivity of silica-embedded titania particles prepared by sol−gel process for the decomposition of trichloroethylene. *Appl. Catal., B* **2000**, *25*, 249−256.
(25) Rubio, J.; Oteo, J. L.; Villegas, M.; Duran, P. Characterization and sintering behaviour of submicrometer titanium dioxide spherical particles obtained by gas-phase hydrolysis of titanium tetrabutoxide. *J. Mater. Sci.* **1997**, *32*, 643−652.
(26) Yasumori, A.; Shinoda, H.; Kameshima, Y.; Hayashi, S. Photocatalytic and photoelectrochemical properties of TiO_2-based multiple layer thin film prepared by sol−gel and reactive-sputtering methods. *J. Mater. Chem.* **2001**, *11*, 1253−1257.
(27) Benfer, S.; Popp, U.; Richter, H.; Siewert, C.; Tomandl, G. Development and characterization of ceramic nanofiltration membranes. *Sep. Purif. Technol.* **2001**, *22*−*23*, 231−237.
(28) Duran, A.; Serna, C.; Fornes, V.; Fernandez-Navarro, J. M. Structural considerations about SiO_2 glasses prepared by sol−gel. *J. Non-Cryst. Solids* **1986**, *82*, 69−77.
(29) Dutoit, D. C. M.; Schmeider, M.; Baiker, A. Titania−silica mixed oxides: 1. Influence of sol−gel and drying conditions on structural properties. *J. Catal.* **1995**, *153*, 165−176.
(30) Schraml-Marth, M.; Walther, K. L.; Wokaun, A.; Handy, B. E.; Baiker, A. Porous silica gels and TiO_2/SiO_2 mixed oxides prepared via the sol−gel process: characterization by spectroscopic techniques. *J. Non-Cryst. Solids* **1992**, *143*, 93−111.
(31) Bacsa, R. R.; Kiwi, J. Effect of rutile phase on the photocatalytic properties of nanocrystalline titania during the degradation of p-coumaric acid. *Appl. Catal., B.* **1998**, *16*, 19−29.
(32) Kiwi, J.; Grätzel, M. Optimization of conditions for photochemical water cleavage. Aqueous Pt/TiO_2 (anatase) dispersions under ultraviolet light. *J. Phys. Chem.* **1984**, *88*, 1302−1307.
(33) Boehm, H. P. Acidic and basic properties of hydroxylated metal oxides surface. *Discuss. Faraday Soc.* **1971**, *52*, 264−275.
(34) Brunauer, S.; Deming, L. S.; Deming, W. E.; Teller, E. On a theory of the van der Waals adsorption of gases. *J. Am. Chem. Soc.* **1940**, *62*, 1723−1732.
(35) IUPAC Manual of Symbols and Terminology, Appendix 2, Pt. 1, Colloid and Surface Chemistry. *Pure. Appl. Chem.* **1972**, *31*, 578.
(36) Sene, J. J.; Zeltner, W. A.; Anderson, M. A. Fundamental photoelectrocatalytic and electrophoretic mobility studies of TiO_2 and V-doped TiO_2 thin-film electrode materials. *J. Phys. Chem. B* **2003**, *107*, 1597−1603.

Received for review January 17, 2006. Revised manuscript received July 31, 2006. Accepted July 31, 2006.

ES060092D